Biophysical Journal Volume 70 April 1996 1796–1802

Immuno-Atomic Force Microscopy of Purple Membrane

Daniel J. Müller,*‡ Cora-Ann Schoenenberger,* Georg Büldt,‡ and Andreas Engel*
*M. E. Müller Institute for Microscopic Structural Biology, Biozentrum University of Basel, CH-4056 Basel, Switzerland, and
‡Forschungszentrum Jülich, IBI-2, Structural Biology, D-52425 Jülich, Germany

ABSTRACT The atomic force microscope is a useful tool for imaging native biological structures at high resolution. In analogy to conventional immunolabeling techniques, we have used antibodies directed against the C-terminus of bacteriorhodopsin to distinguish the cytoplasmic and extracellular surface of purple membrane while imaging in buffer solution. At forces ≥0.8 nN the antibodies were removed by the scanning stylus and the molecular topography of the cytoplasmic purple membrane surface was revealed. When the stylus was retracted, the scanned membrane area was relabeled with antibodies within 10 min. The extracellular surface of purple membrane was imaged at 0.7 nm resolution, exhibiting a major and a minor protrusion per bacteriorhodopsin monomer. As confirmed by immuno-dot blot analysis and sodium dodecyl sulfate-gel electrophoresis, labeling of the purple membrane was not observed if the C-terminus of bacteriorhodopsin was cleaved off by papain.

INTRODUCTION

The atomic force microscope (AFM) (Binnig et al., 1986) allows the surface of biological specimens to be imaged at high resolution under physiological conditions. This has been demonstrated with purple membrane (Butt et al., 1990, 1991), cholera toxin (Yang et al., 1993; Shao and Yang, 1995), gap junctions (Hoh et al., 1993), hexagonally packed intermediate layer (Karrasch et al., 1993, 1994), and OmpF porin (Schabert et al., 1995). Recently individual polypeptide loops connecting transmembrane α-helices of bacteriorhodopsin have been imaged with the AFM (Müller et al., 1995b). Reversible force-dependent structural changes of bacteriorhodopsin molecules were observed at subnanometer resolution and were interpreted as the bending of a single loop (Müller et al., 1995a).

When used to observe the sample by light and electron microscopy, immunolabeling techniques have provided a wealth of structural information at the cellular, supramolecular, and molecular levels. Using purple membrane, we demonstrate that the AFM can be used correspondingly with the additional advantage that after identification in their native environment, the surfaces of biological molecules can be imaged at submolecular resolution. Purple membrane is a highly ordered, two-dimensional (2D) trigonal crystal of lipids and bacteriorhodopsin trimers. Its structure has been solved by high-resolution cryo-electron microscopy (Henderson et al., 1990). We used antibodies directed against the C-terminus of bacteriorhodopsin (Wölfer et al., 1988) to distinguish the surfaces of purple membrane. The specificity of the molecular recognition was demonstrated by the absence of labeling after enzymatic cleavage of the epitope. After the antibodies were removed with the AFM stylus, the submolecular structure of the unveiled cytoplasmic membrane revealed doughnut-shaped trimers, corroborating our previous assignment of the cytoplasmic surface topography of bacteriorhodopsin (Müller et al., 1995a,b).

Received for publication 7 November 1995 and in final form 27 December 1995.

Address reprint requests to Dr. Andreas Engel, M. E. Müller Institute for Microscopic Structural Biology, Biozentrum, University of Basel, Klingelbergstrasse 70, CH-4056 Basel, Switzerland. Tel.: 0041-61-267-2261; Fax: 0041-61-267-2259; E-mail: aengel@ubaclu.unibas.ch.

0006-3495/96/04/1796/07 $2.00

MATERIALS AND METHODS

Sample preparation

Purple membranes were isolated from *Halobacterium salinarium* (ET 1001) as described by Oesterhelt and Stoeckenius (1974). Purple membrane stock solution (10 mg/ml in double destilled water) was diluted 200-fold in 150 mM KCl and 100 mM Tris at pH 9.2. A 25-μl drop of this solution was deposited on freshly cleaved muscovite mica discs (20 mm in diameter) that had been glued onto 25-mm magnetic discs. After 10 to 30 min, the sample was gently washed with buffer to remove membranes that were not firmly attached to the substrate.

Labeling of purple membrane with C-terminus-specific antibodies (Wölfer et al., 1988) was carried out after the membranes were adsorbed to the mica. Antiserum (protein concentration 1 mg/ml) was diluted 500-fold in 150 mM KCl, 100 mM Tris, pH 7.4 or 9.2. A 25-μl drop of this solution was then deposited on the purple membrane-coated mica. After 2 h (or 4 h or 24 h) at 20°C, the sample was mounted in the AFM without washing.

Papain proteolysis

Bacteriorhodopsin was digested with papain type IV (Sigma) as described by Fimmel et al. (1989). Briefly, 0.1 mg/ml papain in 1 mM EDTA, 0.6 mM 2-β mercaptoethanol, 5 mM cysteine-HCl, pH 7.0 (activation buffer), was incubated for 30 min at room temperature. Bacteriorhodopsin (100 μg in 100 μl activation buffer) was digested while shaking at 37°C with 5 μl activated papain for 1 or 2 h. Control samples were treated identically, except that papain was omitted. Digestion was stopped by adding phenylmethylsulfonyl fluoride to a final concentration of 0.1% and 1 ml of 1 M NaCl, 10 mM Tris, pH 6.8. To remove papain, purple membrane were washed twice with 1 M NaCl, 10 mM Tris-HCl, pH 6.8, and collected by centrifugation at 165,000 × g for 20 min at 4°C. Finally, the pellet was resuspended in water and the protein concentration was determined from the OD, using a molar absorption coefficient of 63,000 M^{-1} cm^{-1} at 570 nm (Rehorek and Heyn, 1979) and a molecular weight of 26,000.

SDS-PAGE

Aliquots of untreated, mock-digested, and papain-digested bacteriorhodopsin were subjected to electrophoresis on 15–20% SDS polyacrylamide gradient gels containing 3.2 M urea according to a protocol by Ikeuchi and Inoue (1988).

ECL dot immunobinding

Twofold serial dilutions of protein were applied as 1-μl dots to nitrocellulose membranes (Schleicher and Schüll, Dassel, Germany) starting at 0.03 mg/ml, and were air dried. Unspecific binding sites were blocked by incubating membrane strips with 5% milk powder in phosphate-buffered saline (Dulbecco's formula) containing 0.1% Tween-20 (PBS-Tween) for 30 min at room temperature. Assay strips were then incubated with a 1:5000 dilution of antiserum in PBS-Tween. After 2 h, the membrane strips were washed with 5% milk powder in PBS-Tween, with PBS-Tween, and with 1% "blocking reagent" (Boehringer Mannheim, Germany) in PBS-Tween. Subsequently, they were incubated overnight at 4°C with a 1:5000 diluted goat anti-rabbit antibody conjugated to horseradish peroxidase (Sigma). The immunocomplexes were detected by enhanced chemoluminescence (ECL), using detection reagents from Amersham. After incubation of the nitrocellulose membrane with the detection reagents, the luminescence was immediately recorded on autoradiography film (Kodak X-OMAT XAR-5).

Atomic force microscopy

After the purple membranes were adsorbed to mica, the sample was mounted on the piezo scanner of the atomic force microscope (Nanoscope III; Digital Instruments, Santa Barbara, CA), which was equipped with a liquid cell. Cantilevers with nominal force constants of $k = 0.094$ N/m or $k = 0.022$ N/m and oxide sharpened Si_3N_4 tips were purchased from Olympus (Tokyo, Japan). After several hours of thermal relaxation, the drift of the cantilever deflection angle was at a minimum. Initial engagement of the tip was then performed by setting the scan size to zero to minimize specimen deformation or tip contamination. Before scanning the sample, the operating point of the microscope was set to forces below 0.5 nN.

At low magnification (frame size approximately 600 nm) images were recorded in the error signal mode acquiring the deflection and height signals simultaneously. The deflection signal was minimized by optimizing gains and scan speed. The scan speed was roughly linear to the scan size, 4 to 8 lines per second for lower magnifications (frame size 0.35 to 13 μm) and 8 to 9.6 lines per second for higher magnifications (frame sizes 80 to 130 nm). Thus, for high-resolution imaging the maximum speed (1.25 μm/s) was below the critical scan speed of approximately 2 μm/s (Butt et al., 1993). At high magnification, the deformation of the sample (Weisenhorn et al., 1993) was monitored and minimized by comparing the height profiles acquired in trace and retrace direction, and at different scan angles. The applied force was corrected manually to compensate for the thermal drift of the microscope.

The "D" and "J" piezoscanners used had a scan range of 15 μm and 120 μm. Calibration of the scanners was carried out using layered crystals such as mica (Bailey, 1984) and transition metal dichalcogenides (Wilson and Yoffe, 1969) as substrate references. The lateral calibration was carried out by comparing the lattice constants of the layered surface, and for calibration in the z-direction, defects (large holes or steps) were used (Jungblut et al., 1992).

Image processing

Micrographs (size 512 × 512 pixels) of the purple membranes were selected by crystal order and by comparing the simultaneously monitored height profiles acquired in trace and retrace directions. For image processing, the raw data were transferred to a VAX 3100 workstation and analyzed using the Semper image-processing system (Saxton et al., 1979). Residual lattice disorder was eliminated by correlation averaging (Saxton and Baumeister, 1982). Finally, correlation averaged unit cells were threefold symmetrized.

RESULTS

Biochemical characterization of the carboxyl-terminal region of bacteriorhodopsin

The limited proteolysis of bacteriorhodopsin by papain is shown in Fig. 1 *a*. Intact bacteriorhodopsin migrates on the SDS gel with an apparent molecular mass of approximately 26 kDa. Additional bands indicate that precursor bacteriorhodopsin is processed after incorporation into the membrane in a two-step mechanism via an intermediate product (Wölfer et al., 1988). After a 1-h digestion with papain at a low enzyme-to-substrate ratio (1:200), the prominent protein species migrated with a slightly increased electrophoretic mobility. The migration differences between mature and precursor bacteriorhodopsin remained constant after digestion by papain. According to the folding model of bacteriorhodopsin (Fig. 1 *b*), cleavage under these conditions occurs primarily between Gly-231 and Glu-232 (Liao and Khorana, 1984; Fimmel et al., 1989), shortening bacteriorhodopsin by 17 amino acids at the C-terminus. Digestion for 2 h did not produce additional bacteriorhodopsin fragments.

Evidence that papain digestion had effectively cleaved off the C-terminus is provided by the dot immunobinding experiment shown in Fig. 2. In this experiment a rabbit antibody that recognizes the carboxyl-terminal region of denatured bacteriorhodopsin (Wölfer et al., 1988) was used. Dots of comparable size representing twofold serial dilutions of undigested and digested native bacteriorhodopsin were adsorbed to nitrocellulose membrane. Incubation of the membrane followed by immunodetection revealed that the antibody binds to full-length, native bacteriorhodopsin (*lanes 1* and *2*). After papain digestion for 1 (*lane 3*) and 2 h (*lane 4*), respectively, the cleaved bacteriorhodopsin peptide fragment is no longer recognized by the specific antibody.

Labeling of purple membrane and surface identification

AFM images of native purple membrane adsorbed to freshly cleaved mica recorded in buffer solution at pH 9.2 revealed smooth and flat membrane patches with diameters of up to 2 μm (Fig. 3 *A*), and a thickness of 5.6 ± 0.1 nm (Müller et al., 1995b). At low magnification, no topographic difference between individual membranes was detected, and the free mica surface was atomically flat. After addition of antibodies to adsorbed purple membrane, approximately 30% of the membranes were textured (Fig. 3 *B*), whereas others remained as smooth as the membranes shown in Fig. 3 *A*. Antibodies also adsorbed to the mica surface (Yang et al., 1994) but were swept away by scanning the surface at

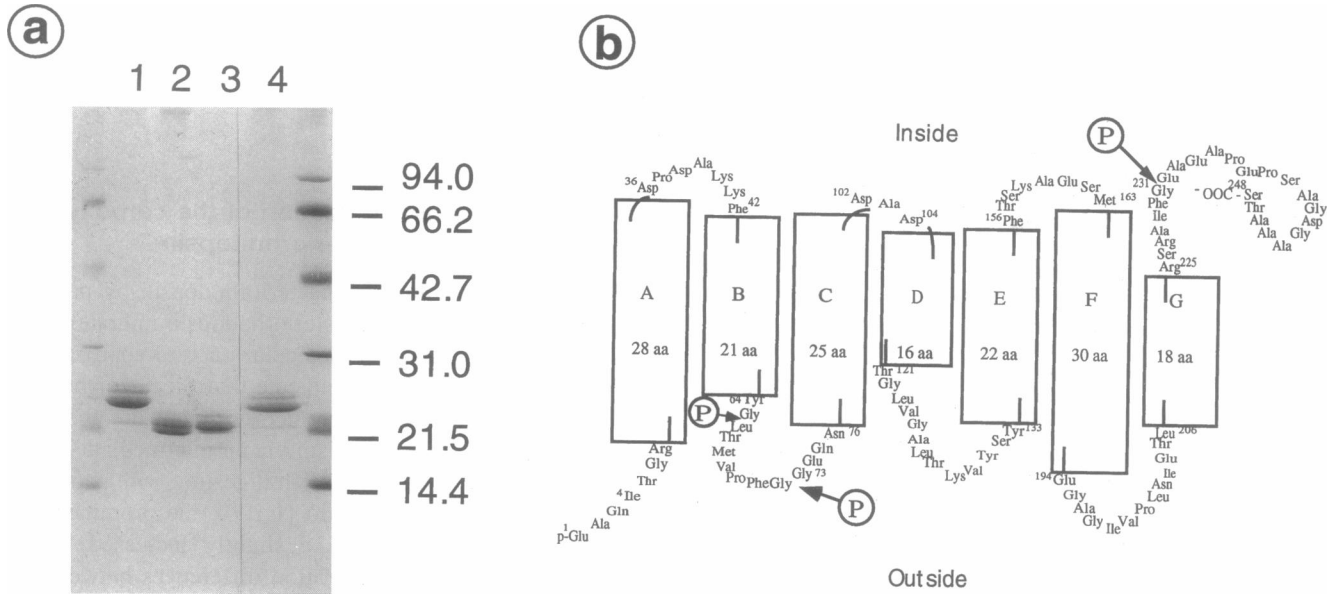

FIGURE 1 (*a*) Analysis of native (*lane 1*), papain digested (*lane 2*, 2 h; *lane 3*, 1 h) and mock incubated (*lane 4*) purple membrane on SDS-PAGE gel. The three protein bands per lane indicate that the precursor of bacteriorhodopsin is processed in two steps via an intermediate product (Wölfer et al., 1988). Marker lane standards (Bio-Rad): phosphorylase b, 94 kDa; bovine serum albumin, 66.2 kDa; ovalbumin, 42.7 kDa; carbonic anhydrase, 30 kDa; soybean trypsin inhibitor, 31 kDa; lysozyme, 14.4 kDa. (*b*) Folding model of bacteriorhodopsin according to the digestion studies of Fimmel et al. (1989). The height of the rectangular columns A to G represent the length of the amino acid chain (aa) if arranged in an α-helical conformation. The arrows indicate the bonds cleaved by papain treatment. The loop connecting α-helices B and C is cut if the incubation time with papain is long enough (Abdulaev et al., 1978; Fimmel et al., 1989), resulting in fragments between 10 and 17 kDa.

forces above ~0.25 nN. Neither increasing the concentration of the antibodies nor increasing the incubation time altered the texture or the fraction of decorated membranes.

Papain-digested purple membrane adsorbed to mica in a manner similar to that of the native purple membrane and exhibited the same dimensions and smooth surface texture (Fig. 3 *C*). Consistent with the absence of antibody binding in the dot immunobinding assay, we did not observe a decoration of the digested membranes (Fig. 3 *D*), even after extending the incubation time with the antibodies to 24 h. These results indicate that purple membranes were specifically labeled by the antibodies directed to the C-terminus when the extracellular surface was in contact with the mica. Thus, the smooth, unlabeled purple membranes exposed their extracellular surface toward the scanning stylus.

High-resolution images of unlabeled membranes

In the low-magnification image displayed in Fig. 3 *B*, the labeled purple membranes were easily distinguished from the unlabeled membranes. A high-magnification image of the unlabeled, extracellular surface (Fig. 4 *A*) revealed the arrangement of triple protrusions on a trigonal lattice ($a = b = 6.2 \pm 0.2$ nm; $n = 200$). The power spectrum (Fig. 4 *B*) exhibited characteristic strong second-order spots, whereas higher orders extended all the way out to the Nyquist cutoff at $(0.7\ \text{nm})^{-1}$. Averaged topographies of images recorded in trace or retrace directions (Fig. 4, *C* and *E*, respectively) showed the tripartite morphology. There were no apparent differences between the trace (Fig. 4 *C*) and the retrace (Fig. 4 *E*) scan directions, indicating that the friction forces were minimal. Enhanced by threefold symmetrization (root-mean-square deviation 8.9%), the correlation averages (Fig. 4, *D* and *F*) revealed three major domains of height 0.22 ± 0.02 nm arranged on an equilateral triangle of 2.9 nm side length, and three minor domains of height 0.08 ± 0.02 nm separated by 1.9 nm. The major trimer had its baseline almost parallel to the lattice lines, and the minor trimer was rotated anti-clockwise by 12.7°.

Structural identification of labeled membranes

A densely labeled purple membrane imaged in buffer solution at low magnification and a force of 0.25 ± 0.05 nN remained textured for several scans, whereas antibodies adsorbed to mica were swept away (Fig. 5 *A*). When the force applied to the stylus was increased to 0.8 nN, antibodies were removed from the purple membrane as well (Fig. 5 *B*). Imaged at high magnification (Fig. 5 *C*), a previously labeled membrane exhibited the donut-shaped bacteriorhodopsin trimers with a corrugation of 0.4 nm (Müller et al., 1995a,b). Often the tip was contaminated after dislodging the antibodies from the membrane and thus was no longer suitable for achieving high-resolution images. When the stylus was withdrawn from the sample for 10 min, the cytoplasmic surface of purple membrane was found to be relabeled with antibodies present in the buffer solution (Fig. 5 *D*), as indicated by the increased surface

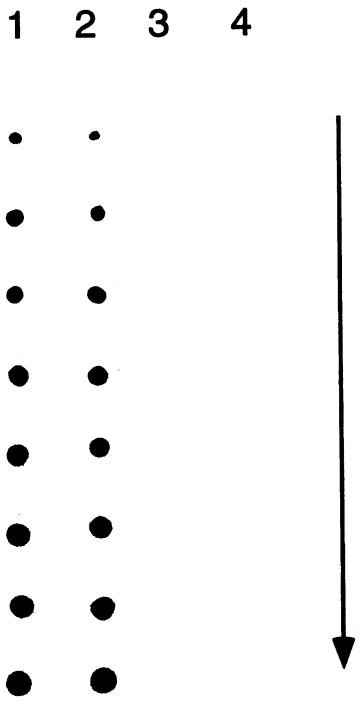

FIGURE 2 Immunodetection of antibody binding to purple membrane. *Lanes 1, 2, 3,* and *4* represent native, mock incubated, 1-h and 2-h papain-digested purple membrane, respectively. Aliquots of twofold serial dilutions of the purple membrane in buffer were applied to nitrocellulose membranes and incubated with antibodies directed against the C-terminus of bacteriorhodopsin. Antibody binding was detected by horseradish peroxidase-conjugated IgG and subsequent enzymatic reaction. As visible in these series, the antibodies bind to native, but not to digested bacteriorhodopsin.

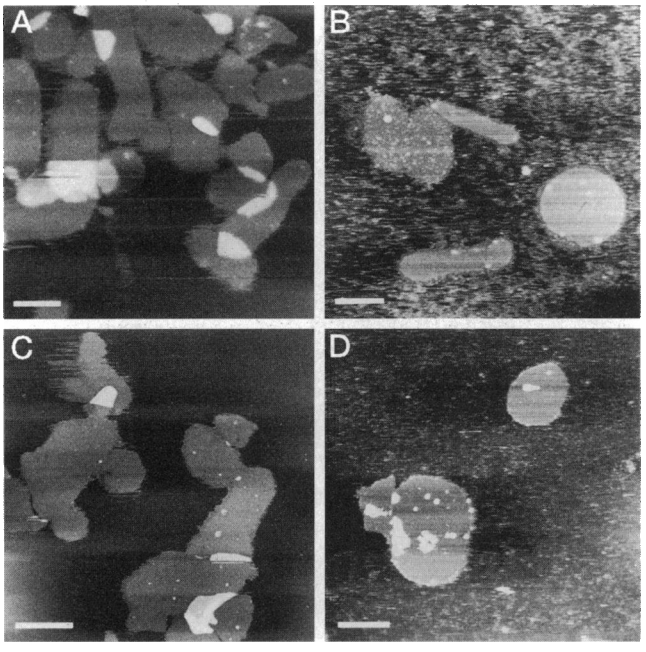

FIGURE 3 Immuno-atomic microscopy of purple membrane. (*A*) Native purple membranes adsorbed flatly onto freshly cleaved mica under optimized buffer conditions (150 mM KCl, 10 mM Tris, pH 9.2). (*B*) Antibodies added to the buffer solution after adsorption of the native membranes yielded some densely labeled membranes, whereas others remained unlabeled. The ratio of textured to bare membranes was 1:2. The antibodies adsorbed to the mica were swept away by applying forces above ~0.25 nN. The loading force for both images was between 0.1 and 0.2 nN, and the scan frequency was 3.5 Hz. (*C*) Papain-digested purple membranes exhibit an adhesion behavior similar to that of native membranes. (*D*) After incubation with antibodies, digested purple membranes remained untextured even after extending the reaction time to 24 h at room temperature. Loading forces were between 0.1 and 0.2 nN at a scan frequency of 3.5 Hz. Scale bars, 500 nm.

corrugation. As displayed at lower magnification, the mica surface of the previous scan had been swept clean, whereas the purple membrane remained decorated (Fig. 5 *E*). These observations suggest a specific binding of antibodies to the cytoplasmic surface of purple membrane.

DISCUSSION

Immunolabeling is a powerful tool for identifying proteins on gels and visualizing their location within cells by light microscopy using fluorescent antibodies or with the electron microscope. In the latter case, small gold particles of a defined size that are conjugated to immunoglobulin G (IgG) or to Fab fragments (Hainfeld, 1988; Baschong and Wrigley, 1990) have been used as markers of thin sections and of negatively stained or unstained samples. Alternatively, negatively stained samples of whole IgG molecules bound to oligomeric complexes allowed subunits and sequence motifs to be located and identified (Stöffler and Stöffler-Meilicke, 1984; Grziwa et al., 1992; Martin et al., 1994). Furthermore, Fab fragments have been used to identify the constituents of periodic arrays (Buhle and Aebi, 1984; Kubalek et al., 1987). In contrast to light microscopy, where the resolution is limited to some fractions of a micrometer, the resolution achieved by electron microscopy is limited by the size of the immunolabel, even when Fab fragments are used (Hainfeld, 1988). However, sample preparation for electron microscopy does not allow molecules to remain in their native state or environment, whereas immunofluorescence microscopy in living cells has been demonstrated (Burke and Warren, 1984).

As presented here, the AFM allows the binding of antibodies to be monitored without the requirement of invasive preparation steps. Our results further demonstrate that antibodies bind specifically and repetitively to the membrane surface and that the underlying protein topography can be imaged at high resolution after antibodies have been removed. Based on this structural fingerprint it is possible to identify the protein to which the antibody binds. This direct assessment relies on the ability of the AFM to image protein surfaces under native conditions (Drake et al., 1989). Topographs of antibodies bound to the S-layer of *Bacillus sphaericus* (Ohnesorge et al., 1992) and of Fab-lipids (Egger et al., 1990) recorded in buffer solution have been

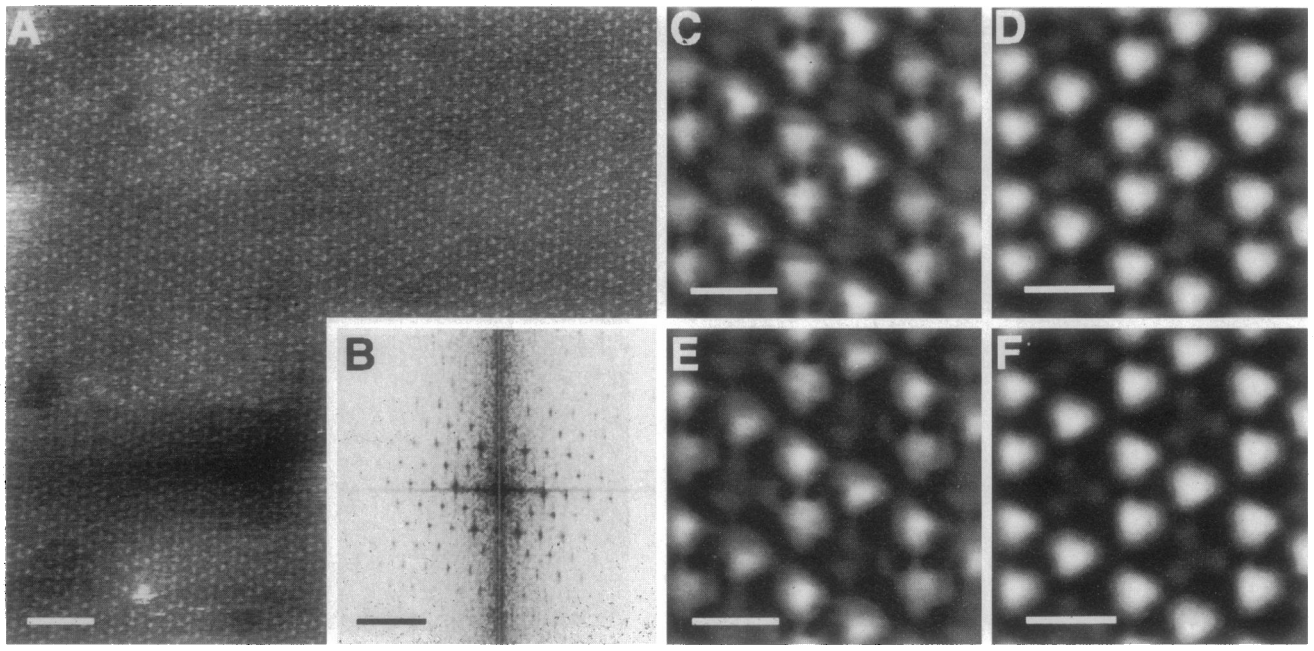

FIGURE 4 High-resolution topography of the extracellular (unlabeled) surface of native purple membrane. (*A*) Membrane recorded in trace (*left to right*) scan direction. (*B*) The diffraction orders extend beyond a resolution of 0.7 nm. Correlation averages of pictures recorded in trace and retrace direction calculated from 770 unit cells are shown in *C* and *E*, respectively. The symmetrized averages *D* and *F* resulted from the averaged topography shown in *C* and *E*. They exhibited a root-mean-square deviation from threefold symmetry of 8.9% and 8.2%, respectively. The height of both topographs was 0.2 nm. Purple membranes were adsorbed and imaged in buffer solution (150 mM KCl, 10 mM Tris; pH 9.2). Scale bars, 20 nm, 2 nm^{-1}, and 4 nm in *A*, *B*, and *C–F*, respectively.

reported, but these experiments have not been further developed.

In our experiments native purple membranes were attached to freshly cleaved mica under conditions previously established to achieve subnanometer resolution (Müller et al., 1995b). Subsequent incubation of the adsorbed membranes with highly specific polyclonal antibodies directed against the C-terminus of bacteriorhodopsin (Wölfer et al., 1988) lead to the decoration of some membranes, whereas others remained unlabeled. As demonstrated by SDS-PAGE, enzymatic digestion of purple membrane with papain resulted in a smaller peptide that was no longer recognized by the antibody in dot-immunobinding experiments (Figs. 1 and 2). Consistent with the absence of the epitope after papain cleavage, antibody labeling was absent in AFM images of cleaved purple membrane (Fig. 3). Even after prolonged incubation with the antibody, the topographs were comparable to those of native, unlabeled purple membrane. This provided solid evidence that the observed decoration of purple membrane is the result of antibody binding.

Antibodies bound to membranes that exposed their cytoplasmic surface, and adsorbed to mica. Whereas antibodies were swept away from the mica at a load of 0.2–0.3 nN, vertical forces close to 1 nN were required to entirely displace the antibodies bound to the purple membrane. The latter forces are significantly larger than the interaction forces of streptavidin-biotin complexes (Florin et al., 1994), indicating that the friction force rather than the vertical force disrupted antibody-antigen interactions in our experiments. Areas cleared by the scanning stylus were rapidly relabeled, demonstrating that the cytoplasmic surface retained its native antigenicity in spite of the contact with the stylus. The underlying cytoplasmic surface also retained the structural features previously observed (Müller et al., 1995b), although the topographs exhibited a slightly lower resolution (Fig. 3). A likely cause for the lower resolution is the deterioration of the tip during removal of the antibodies.

In spite of imaging at 100 pN vertical force, no high-resolution images of antibodies bound to purple membrane could be recorded, although such high-resolution images have been achieved on dried samples with cryo-AFM (Han et al., 1995). Instead, blobs of appropiate dimension were observed (data not shown; Yang et al., 1994). In addition, the texture of labeled cytoplasmic surfaces did not show any regularity. These findings are not surprising. First, IgG molecules are bulky, extending over more than two unit cells and protruding from the surface by 3–5 nm. Second, attached to a flexible, probably disordered C-terminus, antibodies are not expected to assume an ordered arrangement. Third, immobilized only at this flexible epitope, antibodies have a much larger mobility than the bacteriorhodopsin molecules embedded in the crystal lattice and thus are not amenable to high-resolution imaging with the AFM in buffer solution.

Topographs of the extracellular surface showed one major and one minor protrusion per bacteriorhodopsin monomer. Accordingly, a major trimeric protrusion extending

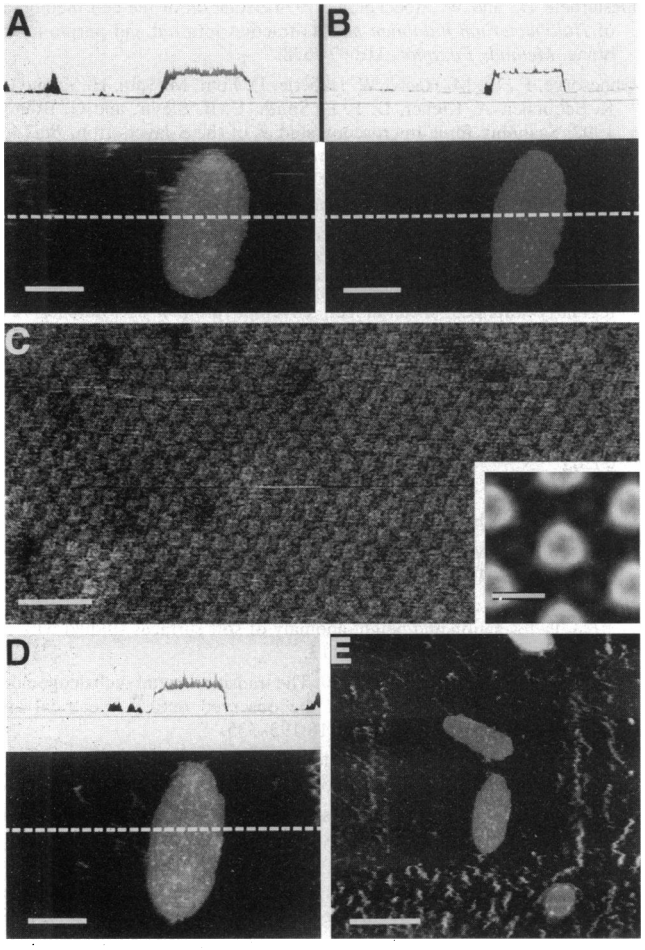

FIGURE 5 Removal of antibodies from the purple membrane surface. (*A*) AFM image of a labeled purple membrane in buffer solution containing antibodies. The topograph was recorded at a loading force of 0.2 nN. A fraction of the antibodies adsorbed to the mica were already swept away by the stylus. (*B*) Same area imaged at a force of about 0.8 nN. The antibodies were completely removed from the substrate and partially from the membrane. (*C*) High-resolution image of the cytoplasmic surface recorded at a force of about 0.25 nN after antibodies were removed. (*D*) Image of the membranes after the stylus has been withdrawn for 10 min recorded at 0.2 nN. The membranes were relabeled by antibodies from the buffer solution. (*E*) Same area imaged at lower magnification and a force of 0.15 nN. The area scanned before can be clearly discerned from the surrounding substrate. Scale bars, 500 nm, 20 nm, 500 nm, and 750 nm in *A–B*, *C* (*inset*, 4 nm), *D*, and *E*, respectively.

0.22 nm above the lipid bilayer and a minor one of 0.08 nm height can be discerned (Fig. 4). Of six possible orientations of this surface conformation two were found to exhibit a good correlation with the 3D structure derived by electron microscopy (Henderson et al., 1990). They have in common that the major protrusion coincides with the short α-helical domain at the extracellular bacteriorhodopsin surface (Henderson et al., 1990), whereas the smaller protrusion is close to the N-terminal helix A.

We conclude that the experiments reported here identify the cytoplasmic and extracellular surfaces of purple membrane. The relatively strong binding of antibodies to the C-terminus of bacteriorhodopsin allows contact mode imaging with the AFM. By monitoring a transient antigen-antibody reaction, the AFM provides the means to first identify biomolecules at the surface of supramolecular assemblies without perturbing the native conformation and subsequently image these structures at high resolution. A prerequisite for immuno-AFM is that the surface corrugation of unlabeled biological systems be within certain limits such that an increase resulting from antibody binding can be detected.

We are grateful to Dr. P. Wrede for supplying the antiserum and thank Dr. S. Müller for critical reading of the manuscript.

DJM was supported in part by grant SFB 189 from the Deutsche Forschungsgemeinschaft. This work was supported by the Swiss National Foundation for Scientific Research (grant 31-424335.94 to AE) and the Maurice E. Müller Foundation of Switzerland.

REFERENCES

Abdulaev, N. G., M. Y. Feigina, A. V. Kiselev, Y. A. Ovchinnikov, L. A. Drachev, A. D. Kaulen, L. V. Khitrina, and V. P. Skulachev. 1978. Products of limited proteolysis of bacteriorhodpsin generate a membrane potential. *FEBS Lett.* 90: 190–194.

Bailey, S. W. 1984. Micas. *Rev. Mineral.* 13.

Baschong, W., and N. G. Wrigley. 1990. Small colloidal gold conjugated to Fab fragments or to immunoglobulin G as high-resolution labels for electron microscopy: a technical overview. *J. Electron Microsc. Tech.* 14:313–323.

Binnig, G., C. F. Quate, and C. Gerber. 1986. Atomic force microscope. *Phys. Rev. Lett.* 56:930–933.

Buhle, E. L., and U. Aebi. 1984. Specific labeling of protein domains with antibody fragments. *J. Ultrastruct. Res.* 89:165–178.

Burke, B., and G. Warren. 1984. Microinjection of mRNA coding for an anti-golgi antibody inhibits intracellular transport of a viral membrane protein. *Cell.* 36:847–856.

Butt, H.-J., K. H. Downing, P. K. Hansma. 1990. Imaging the membrane protein bacteriorhodopsin with the atomic force microscope. *Biophys. J.* 58:1473–1480.

Butt, H.-J., C. B. Prater, and P. K. Hansma. 1991. Imaging purple membranes dry and in water with the atomic force microscope. *J. Vac. Sci. Technol.* B9(2):1193–1197.

Butt, H.-J., P. Siedle, K. Seifert, K. Fendler, T. Seeger, E. Bamberg, A. L. Weisenhorn, K. Goldie, and A. Engel. 1993. Scan speed limit in atomic force microscopy. *J. Microsc.* 169:75–84.

Drake, B., C. B. Prater, A. L. Weisenhorn, S. A. C. Gould, T. R. Albrecht, C. F. Quate, D. S. Cannell, H. G. Hansma, and P. K. Hansma. 1989. Imaging crystals, polymers, and processes in water with the atomic force microscope. *Science.* 243:1586–1588.

Egger, M., F. Ohnesorge, A. L. Weisenhorn, S. P. Heyn, B. Drake, C. B. Prater, S. A. C. Gould, P. K. Hansma, and H. E. Gaub. 1990. Wet lipid-protein membranes imaged at submolecular resolution by atomic force microscopy. *J. Struct. Biol.* 103:89–94.

Fimmel, S., T. Choli, N. A. Dencher, G. Büldt, and B. Wittmann-Liebold. 1989. Topography of surface-exposed amino acids in the membrane protein bacteriorhodopsin determined by proteolysis and microsequencing. *Biochim. Biophys. Acta.* 978:231–240.

Florin, E.-L., T. M. Vincent, and H. E. Gaub. 1994. Adhesion forces between individual ligand-receptor pairs. *Science.* 264:415–417.

Grziwa, A., B. Dahlmann, Z. Cejka, U. Santarius, and W. Baumeister. 1992. Localization of a sequence motif complementary to the nuclear localization signal in proteasomes from *Thermoplasma acidophilum* by immunoelectron microscopy. *J. Struct. Biol.* 109:168–175.

Han, W. H., J. X. Mou, J. Sheng, J. Yang, and Z. F. Shao. 1995. Cryo atomic force microscopy: a new approach for biological imaging at high resolution. *Biochemistry.* 34:8215–8220.

Hainfeld, J. F. 1988. Gold cluster-labelled antibodies. *Nature.* 333: 281–282.

Henderson, R., J. M. Baldwin, T. A. Ceska, F. Zemlin, E. Beckman, and K. H. Downing. 1990. Model for the structure of bacteriorhodopsin based on high-resolution electron cryo-microscopy. *J. Mol. Biol.* 213: 899–929.

Hoh, J. H., G. E. Sosinsky, J.-P. Revel, and P. K. Hansma. 1993. Structure of the extracellular surface of the gap junction by atomic force microscopy. *Biophys. J.* 65:149–163.

Ikeuchi, M., and Y. Inoue. 1988. A new 4.8 kDa polypeptide intrinsic to photosystem II reaction center, as revealed by modified SDS-PAGE with improved resolution of the low molecular-weight proteins. *Plant Cell Physiol.* 29:1233–1239.

Jungblut, H., S. A. Campbell, M. Giersig, D. J. Müller, and H.-J. Lewerenz. 1992. Scanning tunneling microscopy observations of biomolecules on layered materials. *Faraday Discuss.* 94:183–198.

Karrasch, S., M. Dolder, J. Hoh, F. Schabert, J. Ramsden, and A. Engel. 1993. Covalent binding of biological samples to solid supports for scanning probe microscopy in buffer solution. *Biophys. J.* 65: 2437–2446.

Karrasch, S., R. Hegerl, J. Hoh, W. Baumeister, and A. Engel. 1994. Atomic force microscopy produces faithful high-resolution images of protein surfaces in an aqueous environment. *Proc. Natl. Acad. Sci. USA.* 91:836–838.

Kubalek, E., S. Ralston, J. Lindstrom, and N. Unwin. 1987. Location of subunits within the acetylcholine receptor by electron image analysis of tubular crystals from *Torpedo marmorata. J. Cell. Biol.* 105:9–18.

Liao, M.-J., and H. G. Khorana. 1984. Removal of the carboxyl-terminal peptide does not affect refolding or function of bacteriorhodopsin as a light-dependent proton pump. *J. Biol. Chem.* 259:4194–4199.

Martin, J., K. N. Goldie, A. Engel, and F. U. Hartl. 1994. Topology of the morphological domains of the chaperonin GroEL visualized by immunoelectron microscopy. *Biol. Chem. Hoppe Seyler.* 375:635–639.

Müller, D. J., G. Büldt, and A. Engel. 1995a. Force-induced conformational change of bacteriorhodopsin. *J. Mol. Biol.* 249:239–243.

Müller, D. J., F. A. Schabert, G. Büldt, and A. Engel. 1995b. Imaging purple membranes in aqueous solutions at subnanometer resolution by atomic force microscopy. *Biophys. J.* 68:1681–1686.

Oesterhelt, D., and W. Stoeckenius. 1974. Isolation of the cell membrane of *Halobacterium halobium* and its fraction into red and purple membrane. *Methods Enzymol.* 31:667–678.

Ohnesorge, F., W. M. Heckl, W. Häberle, D. Pum, M. Sara, H. Schindler, K. Schlicher, A. Kiener, D. P. E. Smith, U. B. Sleytr, and G. Binnig. 1992. Scanning force microscopy studies of the S-layers from *Bacillus coagulans* E38–66, *Bacillus sphaericus* CCM2177 and of an antibody binding process. *Ultramicroscopy.* 42–44:1236–1242.

Rehorek, M., and M. P. Heyn. 1979. Binding of all-*trans*-retinal to the purple membrane. Evidence for cooperativity and determination of the extinction coefficient. *Biochemistry.* 18:4977–4983.

Saxton, W. O., and W. Baumeister. 1982. The corelation averaging of a regularly arranged bacterial cell envelope protein. *J. Microsc.* 127: 127–138.

Saxton, W. O., T. J. Pitt, and M. Horner. 1979. Digital image processing: the Semper system. *Ultramicroscopy.* 4:343–354.

Schabert, F. A., C. Henn, and A. Engel. 1995. Native *Escheria coli* OmpF porin surfaces probed by the atomic force microscopy. *Science.* 268: 92–94.

Shao, Z., and J. Yang. 1995. Progress in high resolution atomic force microscopy in biology. *Q. Rev. Biophys.* 28:195–251.

Stöffler, G., and M. Stöffler-Meilicke. 1984. Immunoelectron microscopy of ribosomes. *Annu. Rev. Biophys. Bioeng.* 13:303–330.

Weisenhorn, A. L., M. Khorsandi, S. Kasas, V. Gotzos, and H.-J. Butt. 1993. Deformation and height anomaly of soft surfaces studied with an AFM. *Nanotechnology.* 4:106–113.

Wilson, J. A., and A. D. Yoffe. 1969. The transition metal dichalcogenides discussion and interpretation of the observed optical, electrical and structural properties. *Adv. Phys.* 18:193–335.

Wölfer, U., N. A. Dencher, G. Büldt, and P. Wrede. 1988. Bacteriorhodopsin precursor is processed in two steps. *Eur. J. Biochem.* 174:51–57.

Yang, J., J. X. Mou, and Z. F. Shao. 1994. Molecular resolution atomic force microscopy of soluble proteins in solution. *Biochim. Biophys. Acta.* 1199:105–114.

Yang, J., L. K. Tamm, T. W. Tillack, and Z. Shao. 1993. New approach for atomic force microscopy of membrane proteins. *J. Mol. Biol.* 229: 286–290.